J MATER SCI 41 (2006) 937–950

Recent advances on understanding the origin of superhardness in nanocomposite coatings: A critical review

CHUNSHENG LU*, YIU-WING MAI
Centre for Advanced Materials Technology (CAMT), School of Aerospace, Mechanical and Mechatronic Engineering J07, The University of Sydney, Sydney, NSW 2006, Australia
E-mail: chunsheng.lu@aeromech.usyd.edu.au; E-mail: mai@aeromech.usyd.edu.au

YAO-GEN SHEN
Department of Manufacturing Engineering and Engineering Management (MEEM), City University of Hong Kong, Kowloon, Hong Kong, China
E-mail: meshen@cityu.edu.hk

The remarkable mechanical properties of nanocomposite coatings, such as superhardness, high elastic modulus and recovery, excellent resistance against cracking, low wear rate, and high thermal stability, are due to their unique structures and deformation mechanisms at the nanometer scale. In this paper, recent advances are reviewed mainly with respect to the understanding of the origin of superhardness in nanocomposite coatings. A few controversial issues relevant to the identification of superhard coatings are mentioned. Also discussed are several models, based on analyses and simulations at different levels from continuum to atomistic scales, to elucidate likely superhardening mechanisms. Finally, some open problems and continuing challenges are highlighted.

1. Introduction

Recent interest in superhard nanocomposites (defined as those with Vickers hardness $H \geq 40$ GPa; for comparison, diamond with $H = 80$–100 GPa is believed to be the hardest material in nature), especially in the form of thin films or coatings, is mainly driven by their unusual mechanical properties, potentially wide engineering applications in durable machining and forming tools, precision dies/moulds, microelectronic and mechatronic devices, and growing demand for "green production" like dry machining without using any environmentally hazardous coolants [1–10]. Compared to a large number of traditional hard materials such as titanium nitride (TiN), a most widely used hard coating material with $H \approx 20$ GPa, only a few superhard materials are available, e.g., cubic boron nitride (c-BN, $H \approx 50$ GPa), amorphous diamond-like carbon (a-DLC, $H \approx 65$ GPa), and polycrystalline diamond ($H = 70$–80 GPa) [7–10]. Unfortunately, these superhard materials are thermodynamically unstable, which has severely limited the range of their applications. The high solubility of carbon in steel, silicon and other alloys restricts diamond-coated cutting tools to the machining of aluminium and its alloys. Similar problems exist in c-BN-coated cutting tools due to the high chemical affinity of boron to iron [9]. Thus, it is not surprising that many endeavours have been devoted to searching novel superhard materials, especially nanocomposite coatings with superhardness.

Generally speaking, there are two main types of superhard coatings: multilayered (or superlattice) and nanocomposite coatings. Experimental results showed that the overall hardness of multilayered coatings, with individual layers or phases in the range of 5–10 nanometers, is greater than their individual components or those obtained in terms of the rule-of-mixtures. Here, reasons for the hardness enhancement of multilayered coatings are rather complicated and influenced by many factors [11]. Although their hardness is very sensitive to the superlattice period, cutting tools coated with multi-layers have been widely used in commercial products. Nanocomposite coatings, however, are still at the early stage of development, and the origin of

*Author to whom all correspondence should be addressed.
0022-2461
DOI: 10.1007/s10853-006-6577-9

superhardness is far from being understood. In general, a superhard nanocomposite coating comprises two or more phases that are either mutually immiscible and form very fine dispersions of a single phase embedded in a second amorphous phase, such as nanocrystalline TiN and amorphous Si_3N_4 (nc-TiN/a-Si_3N_4), nc-W_2N/a-Si_3N_4, and nc-TiN/a-TiB_2, or contain two nanocrystalline phases, such as nc-TiN/BN, nc-TiN/AlN, etc. [7, 9, 12, 13]. In contrast to c-BN and polycrystalline diamond, nanocomposite coatings are thermodynamically more stable, resistant against oxidation at elevated temperature, and feasible in deposition processes. Meanwhile, they can be readily scaled up from laboratory prototypes to industrial production requirements. Similar strategies were also developed for creating high-hardness and toughened ceramics, by using nanometer-size crystals formed by devitrification of a glass matrix, in which nanocrystalline alumina-rich phases are dispersed throughout the amorphous, non-crystalline glassy matrix [14, 15].

Important progress has been achieved in the past two decades to develop new nano-structured materials in a controlled manner. Nano-structured crystalline composites exhibit mechanical properties that differ significantly from those of their components in bulk forms [16, 17]. It is commonly believed that the remarkable mechanical properties of nanocomposite coatings, such as superhardness, high elastic modulus and recovery, excellent resistance against cracking, low wear rate, and high thermal stability, originate from their peculiar nano-structures and high density of interfaces. However, a better understanding towards intrinsic superhardening mechanisms is still one of the fundamental but yet unsolved subjects. In this paper, recent advances on understanding the origin of superhardness in nanocomposite coatings are critically reviewed. A few controversial issues relating to the identification of superhard coatings and the measurement of hardness are discussed. Several typical models at different scales are introduced to illuminate likely superhardening mechanisms. Finally, some open problems and continuing challenges are highlighted.

2. Pseudo-superhardness and stability

The hardness of a material is usually defined as:

$$H = \frac{P_{\max}}{A} \tag{1}$$

where $P_{\max}$ is the maximum applied load, and A is the surface or projected area of impression. It is obvious to see that, the harder a material the more difficult it is to make an indentation or scratch. Traditional methods of measuring hardness, such as Vickers, Brinell, Knoop, Berkovich, and Rockwell tests, although simple and convenient, involve too many variables to provide a scientific definition of hardness. Hence, there is not an absolute scale for hardness, and the different types of tests measure different things [18 , 19]. For the Vickers test, A is the total surface area of indentation. Thus, the Vickers hardness is approximately equal to the average pressure under an indenter at yielding [20].

2.1. Instrumented indentation

The instrumented depth-sensing indentation technique introduced by Oliver and Pharr [21] has been widely applied in testing mechanical properties, such as elastic modulus, hardness, and fracture toughness of thin films and small volumes of materials, the three fundamental modes of deformation in solids – elasticity, plasticity, and fracture. It provides a direct approach for the identification of superhard nanocomposite coatings, where the number of test variables is reduced to a manageable level and their mechanical properties can be determined directly from indentation load-displacement curves without the need to image the indent impression [22]. However, since there is still a lack of an absolute definition of hardness [23], clarifying the implication of hardness and further superhardening mechanisms is of utmost importance in the search for novel superhard materials.

Using the nanoindentation method to measure the hardness and elastic modulus of a nanocomposite coating, three important quantities must be determined from the load-displacement curves during one cycle of loading and unloading: the maximum load $P_{\max}$, the maximum displacement $h_{\max}$, and the elastic unloading stiffness $S = \mathrm{d}P/\mathrm{d}h$ [21, 22]. Thus, the measurements of hardness and elastic modulus are mainly based on the unloading curve shown schematically in Fig. 1. A typical example of nanoindentation tests on nc-TiN/a-SiN_x coatings with the Si content of 8.6 at.% is shown in Fig. 2 [24]. Although the nanoindentation method has facilitated the measurement of mechanical properties at small scales, it seems not so easy to obtain the intrinsic values of hardness and elastic modulus of nanocomposite coatings since there are many factors that could influence the results. External factors include indenter geometry, tip rounding, test machine compliance etc.; and internal (material-related) factors include pile-up and sink-in, indentation size effect, surface roughness, residual stress, thickness of a coating, substrate etc [20–26]. This has led to claims that superhard or even ultrahard ($H > 70$ GPa) coatings are caused by artifacts in synthesis or measurement [27, 28].

Since there is a very high elastic recovery for superhard nanocomposite coatings, a direct and instructive approach for identifying superhard coatings is to compare the whole indentation curves with those of well-defined materials like diamond. According to the classical Hertzian elastic indentation solution, we have $P \sim h^{3/2}$. In the first approximation, there should be a linear relationship in the log-log plot [29]. For example, the Hertzian plots for di-

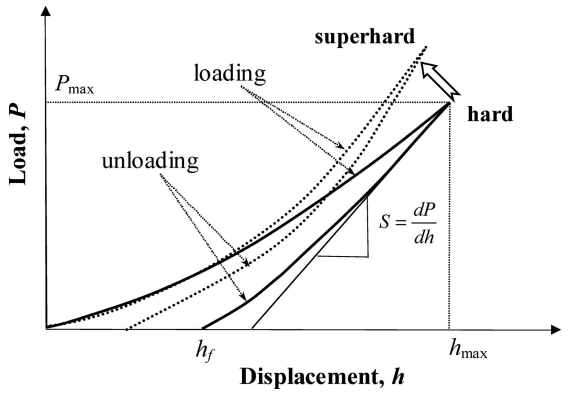

Figure 1 Schematic of indentation load-displacement curves for hard and superhard coatings, where three important parameters are shown. For superhard coatings, the elastic recovery may be up to 80% or even ≥ 90%.

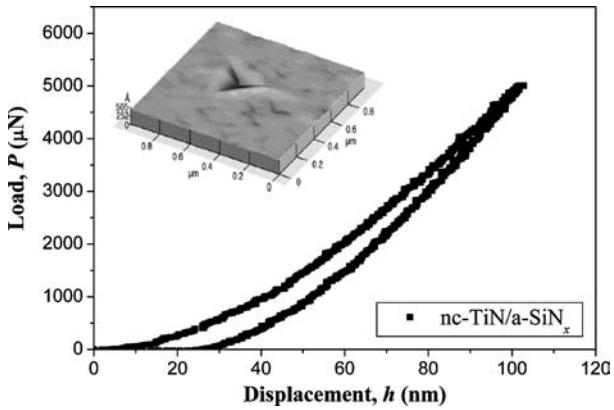

Figure 2 Nanoindentation load-displacement curve from nc-TiN/a-SiN$_x$ coatings with a Si content of 8.6 at.%. The inset is an AFM image after the nanoindentation test [24].

amond and nc-TiN/a-Si_3N_4/a- (or nc-$TiSi_2$) are shown in Fig. 3, where experimental data follow a straight line with slopes of 1.71 and 1.67, respectively [30]. Here, the small difference from the true Hertzian slope, 3/2 = 1.5, can be attributed to the influence of inelastic deformation and geometry of the Vickers indenter.

2.2. Indentation size effect

To avoid the influence of a substrate on the hardness measurement of a coating, the maximum indentation depth should not exceed about 10% of the thickness of the coating according to a rule-of-thumb criterion [31]. Therefore, the so-called indentation size effect, i.e. an increase in hardness with decreasing indentation depth in the submicrometer or nanometer range, has to be considered in the measurement of the intrinsic hardness of a nanocomposite coating. By introducing material scales into a phenomenological model, a strain gradient plasticity model was developed to describe the size effect behavior for crystalline materials [32]. It is noted that large strain gradients inherent in small indentations lead to geometrically necessary dislocations. Using this concept, Nix and Gao [25] obtained the following expression for the increase in hardness H as a function of indentation depth h:

$$\frac{H}{H_0} = \sqrt{1 + \frac{h^*}{h}} \qquad (2)$$

where H_0 is the hardness in the limit of infinite depth and h^* is a characteristic length that depends on the shape of the indenter [25]. As shown in Fig. 4, the indentation size effect on the hardness of nano-structured AlN coatings is fitted well by Equation 2, and the intrinsic hardness value $H_0 = 20.0$ GPa obtained is in good agreement with other tests or calculations [33].

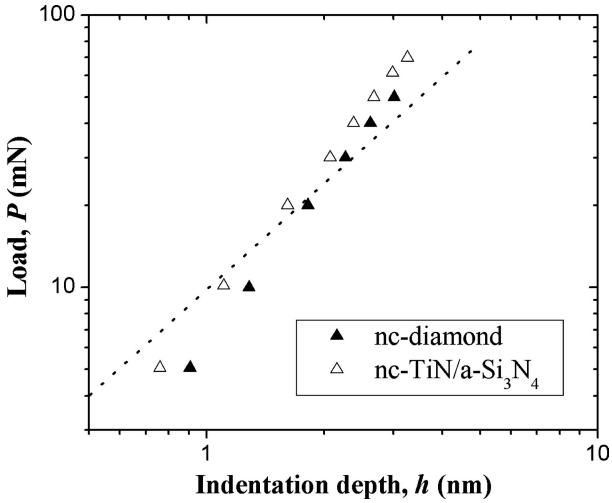

Figure 3 Applied load *versus* indentation depth for nc-TiN/a-Si_3N_4 nanocomposites and nc-diamond, where the dotted line indicates the Hertzian plot with a slope of 3/2. Data from [30].

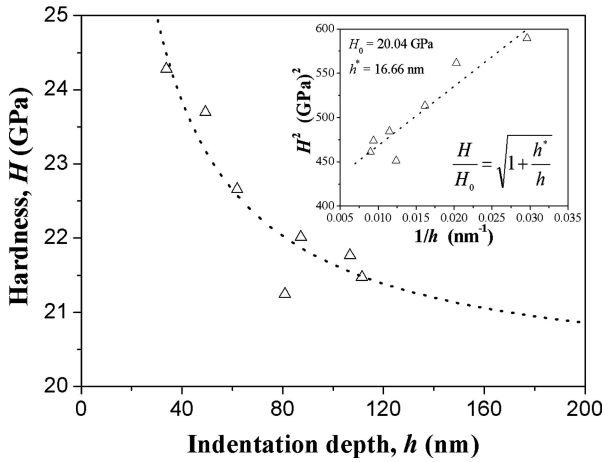

Figure 4 Hardness *versus* indentation depth for AlN thin films, where the dotted line is the best fitting curve by Equation 2. The inset displays the data in a plot of H^2 *vs* 1/h.

It is worth noting that Equation 2 was developed for ductile crystalline materials. It is easy to see that, based on Equation 2, a large value of H_0 would cause h^* to be very small. That is, hardness depends weakly on depth at a given level of indentation. However, a recent study on the nanoindentation tests of Ti-Al-N thin films showed that hardness increases exponentially as the indentation depth decreases [34]. This implies that there exist some new deformation mechanisms rather than dislocation pile-ups, which are responsible for the indentation size effect of superhard nanocomposite coatings. It is also worth noting that the influence of the substrate on hardness exists even if the indentation depth is less than 10% of the thickness of the coatings [35]. In fact, many deposited nanocomposite coatings have significant micro-structural gradients through the thickness of coatings, which also affect the measurement of hardness. Thus, this is still an important problem to be considered in the measurement of their intrinsic hardness since the maximum indentation depth is usually less than several tenths of a micrometer in nano-indentation tests of superhard coatings.

2.3. Residual stress

The influence of residual stress on the hardness and stability of superhard nanocomposite coatings is another important factor mostly considered in fabrication and measurement [36, 37]. The residual stress σ_r can be conveniently evaluated from the measured curvature radius R of a coating using the relationship:

$$\sigma_r = \frac{E}{6(1-\nu)}\frac{t_s^2}{t_c R} \tag{3}$$

where E and ν are elastic modulus and Poisson's ratio of the substrate, t_c and t_s are thickness of the coating and substrate, respectively [38].

There are two main kinds of fabrication method for superhard coatings: chemical vapor deposition (CVD) such as plasma induced techniques; and physical vapor deposition (PVD) such as arc evaporation and reactive magnetron sputtering [9]. Since high temperatures are needed for thermal CVD in the material system like Ti-Si-N, no hardness enhancement has been reported [39]. Conversely, a high biaxial compressive stress is commonly observed in PVD deposited films at a very low sputtering pressure. Thus, the low thermal stability and hardness reduction upon annealing to ≥400°C are due to either the relaxation of a high biaxial compressive stress left in films during deposition or a miscibility of compositions. Fig. 5 shows that superhard coatings can be achieved when the biaxial compressive stress reaches a value of ∼3 GPa or less [40]. This provides an effective superhardening method, but the thermal stability of these nanocomposite coatings is very low. For example, HfB_2 coatings with

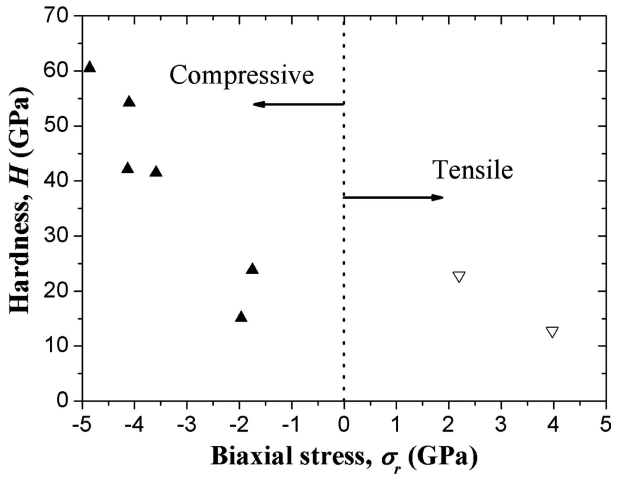

Figure 5 Effects of biaxial compressive/tensile stresses on the hardness of TiN coatings deposited by magnetron sputtering at a low pressure of 0.3 Pa (3×10^{-3} mbar). Data from [40].

hardness 72 GPa deposited at a low pressure of 0.5 Pa have a high compressive biaxial residual stress of ∼7 GPa; upon annealing at 650°C the hardness decreases to 17 GPa [41]. It should be noted that some test results have shown that there is no well-defined correlation between compressive stresses in coatings and observed nano-hardness values [42].

Although residual stress has no effect on its intrinsic hardness of a coating, the apparent or measured values of hardness are affected by the presence of residual stresses, as shown in Fig. 5. In addition, such residual stresses will influence the buckling and delamination of the interface between coating and substrate [43]. To alleviate this problem, Veprek [44] proposed a genetic design concept for superhard nanocomposite coatings based on thermodynamically driven segregation in binary and ternary systems that are stable even at temperatures up to ≥ 1000°C. The condition for spinodal decomposition can be represented by:

$$\frac{\partial^2 \Delta G^0(A_{1-x}B_x)}{\partial x^2} < 0 \tag{4}$$

where ΔG^0 is the free energy of formation of a mixed phase $A_{1-x}B_x$, and x is the composition of phase B (for more details about spinodal decomposition, see [44–46]). The deposited nanocomposite coatings have a small compressive stress less than 1 GPa [3].

3. Modeling and simulation

One of the fundamental principles in materials science is that the mechanical and physical properties of materials are closely related to their structures at various scales. For example, to understand the origin of Young's modulus, we focus on structures at the atomic level. But, for proper-

ties of plasticity and fracture, we focus on the movement of dislocations and defects like cracks and voids at the micro-level. As discussed above, hardness is the ability of one material to resist being scratched or indented by another. Unlike elastic modulus, the origin of hardness and superhardness is not so easily defined at the atomic scale, and there is no unequivocal correlation between elastic modulus and hardness. In fact, hardness is more closely related to the yield strength of a material. For simplicity, we ignore the detail microstructures of grains in a polycrystal and treat it as a continuum. In terms of the upper-bound theorem [47], we have $H = 3\sigma_y$. Generally, $H = (2.6 \sim 3.0)\sigma_y$, where σ_y is the tensile yield strength, and a correction factor is needed for materials with work-hardening. For a harder material, the hardness can be estimated from its yield strength using the Marsh relationship [48]:

$$\frac{H}{\sigma_y} = a + b\frac{3}{3-\lambda}\ln\left(\frac{3}{\lambda + 3\mu - \mu\lambda}\right) \tag{5}$$

where a and b are constants, $\mu = (1+\nu)\sigma_y/E$, $\lambda = 6(1-2\nu)\sigma_y/E$, and ν is Poisson's ratio. An approximate estimation on nc-TiN/a-Si_3N_4 coatings gives: $H_{\max} \approx 0.117E$, where the measured Young's modulus E is approximately 450 to 550 GPa in the region of maximum hardness. Thus, the maximum hardness value of more than 45 GPa can be obtained [42].

It has been shown that the mechanical properties of nanocomposite coatings, such as hardness and abrasive wear-resistance, can be substantially improved owing to the pseudo-plastic deformation caused by nano-grain rotation, complex grain boundary, amorphous structures, and even the formation of intrinsic stresses in thin films etc. Undoubtedly, the question on the origin of superhardness of nanocomposite coatings is very complex, and thus it is necessary to identify the key parameters. According to dimensional analysis (noting that hardness has the dimension of stress) [49, 50], a generalized functional relationship can be written as:

$$\frac{H}{\sigma_y} = f\left(\frac{\sigma_y}{E}, \nu, n, \frac{t}{d}, \ldots\right) \tag{6}$$

where n is a work-hardening exponent, d and t are two characteristic lengths of microstructures at the nano-scale or atomistic-scale, such as the grain size of nano-crystals and the thickness of amorphous boundary. Here, it should be pointed out that the mechanical properties of thin films or coatings may be very different from those of their bulk. Next, we focus our attention on several models in order to illuminate, at various length scales, likely superhardening mechanisms.

3.1. Continuum mechanics models

Intuitively, the structure of superhard nanocomposite coatings at the nanometer scale is still a continuum [51], as shown in Fig. 6. Thus, a natural attempt to understand the origin of super-hardness is based on conventional fracture mechanics scaled down to the dimension of nano-cracks, in combination with a low concentration of possible flaws introduced into a coating during its preparation [30, 46, 52–54]. The latter is a consequence of self-organization due to the thermodynamically driven formation of stable nanostructures.

In the first approximation, let us suppose that there is a nano-crack in the microstructure of a superhard coating like nc-TiN/a-Si_3N_4 formed during the fabrication process or caused by the internal misfit stresses under an applied tensile stress [55]. According to Griffith's energy criterion [56], the critical stress σ_c, which causes the nano-crack to grow, is $\sigma_c \approx \sqrt{E\gamma/a}$, where E is elastic modulus, γ is surface free energy, and a is crack length. Because the size of a nano-crack, in randomly oriented nanocomposites, can be only a fraction of the crystallite grain (about 1–2 nm), the stress concentration factor of such an atomically sharp crack is very low ($2 \sim 4$) and the critical stress needed to propagate the nano-crack can approach an extremely high value. Further, given that the nano-crack opens, the deflection and branching during its growth, due to the obstacle of the nearest neighbor nano-crystals, will

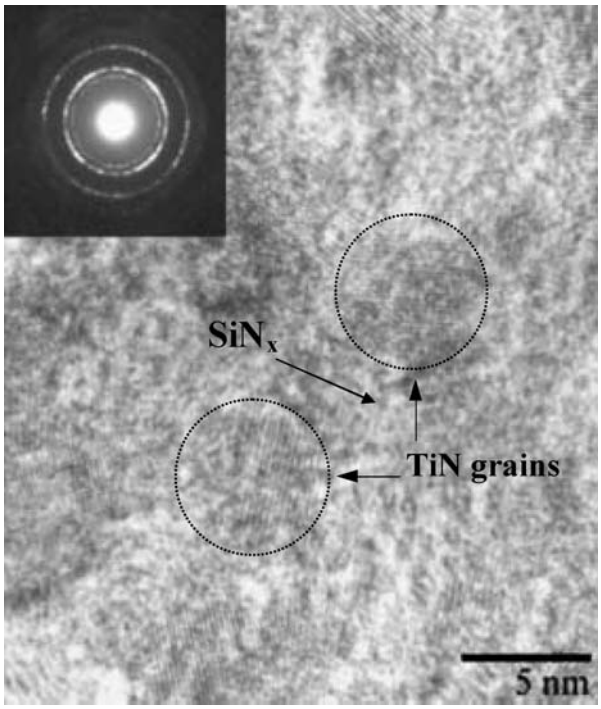

Figure 6 High resolution TEM image of a 50-nm-thick TiN/SiN_x film with a Si content of 11.4 at.% shows that the TiN nanocrystallites are embedded in an amorphous SiN_x matrix, where the inset is the selected area electron diffraction pattern [51].

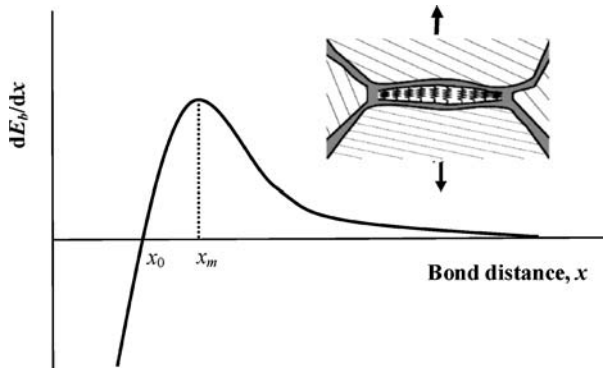

Figure 7 First derivative of binding energy E_b against bond distance x, where x_0 is the equilibrium distance and x_m is the critical distance at which a bond would break. The inset shows the flexing of bonds across the interface between nanocrystals [30].

lead to a reduction of the corresponding stress concentration factor. Thus, the fracture of nano-composites due to the formation and stable growth of nano-cracks seems impossible, and other inelastic deformation mechanisms should be responsible for their high hardness [30].

As shown in Fig. 1, the larger the elastic recovery, the smaller the dissipated energy of plastic deformation and the harder the nanocomposite coatings. The high elastic energy density in superhard nanocomposite coatings can be explained by a mechanism called "reversible non-linear flexing" between nanocrystallites [30, 46]. Fig. 7 shows the universal decohesion curve, that is, the dependence of the restoring force (which is the first derivative of binding energy E_b *versus* bond distance x) on the deformation of interatomic bonds. Here the bond dilation can exceed 10–20% of the equilibrium bond length, which is about the limit of breaking an interatomic covalent bond. Thus, the whole range $0 \leq x < x_m$ corresponds to reversible nonlinear elastic deformation. A simple estimation shows that the energy density of flexing can exceed that of linear elastic deformation of conventional materials by a large factor [52]. However, further work is needed to extend this concept to account for the mechanism of plastic deformation, which is more closely related to hardness.

It is well-known that the yield or flow strength σ_y of polycrystalline materials increases as the grain size d decreases. This is the classic Hall-Petch relationship:

$$\sigma_y = \sigma_0 + kd^{-1/2} \tag{7}$$

where σ_0 is friction stress required to move dislocations in single crystals, and k is a material constant [57,58]. The hardness H of polycrystalline materials follows a similar correlation so that:

$$H = H_0 + kd^{-\beta} \tag{8}$$

where H_0 is hardness of a single crystal or bulk sample, d is average grain size or layer thickness, and β is an exponent between 0 and 1. Numerous experiments have shown that the Hall-Petch relationship is obeyed for coarse-grained materials (down to ~100 nm), which can be described by the dislocation pile-up theory [59]. As grain sizes become smaller, the effect of dislocation blocking, that is, strengthening or hardening the material, increases. Provided that the Hall-Petch relationship was correct in the nanometer range, it is not surprising that nanocrystalline metals or ceramics could be used as candidates for superhard materials. Both experimental and simulation findings indicated that, however, as the grain size is reduced to less than 100 nm, the k values in Equations 7 and 8 tend to decrease and in some cases even become negative, that is, the hardness levels off or decreases at the nano-grain sizes [59–63]. This is the so-called reverse Hall-Petch effect, as illustrated in Fig. 8. As grain sizes approach the nanometer scale, the percentage of grain boundary atoms also increases. For example, in a sample with grain diameters of 20 nm, about 10% of atoms are located at the grain boundaries [64]. In this region, the yield stress increases with the decrease of grain sizes, and a larger applied stress is required because the pile-up contains fewer dislocations. Let us assume that dislocation sources must operate in each grain, an additional component of the yield stress exists of at least Gb/d, where G is the shear modulus and b is Burgers vector. Thus, the yield stress σ_y at the nanometer grain size should rise as d^{-1} [65], much faster than $d^{-1/2}$ as estimated by the Hall-Petch relationship in Equation 7. That is, the mechanism based on dislocation pile-up is no longer operative in such a material and plastic deformation may be carried by atomic sliding in grain boundaries rather than by dislocation motion [59–63].

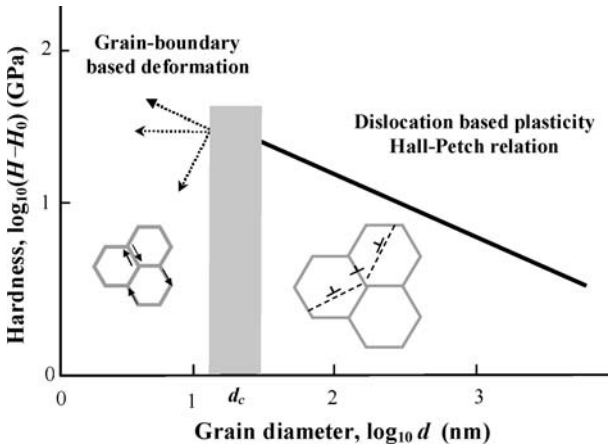

Figure 8 Illustration of hardness or yield strength of a material as a function of grain size, where two regions are revealed in which the deformation is mediated by dislocation pile-up (coarse-grains) and grain boundaries (nano-grains), respectively. The Hall-Petch relation works well for coarse-grained materials, where d_c is a critical length.

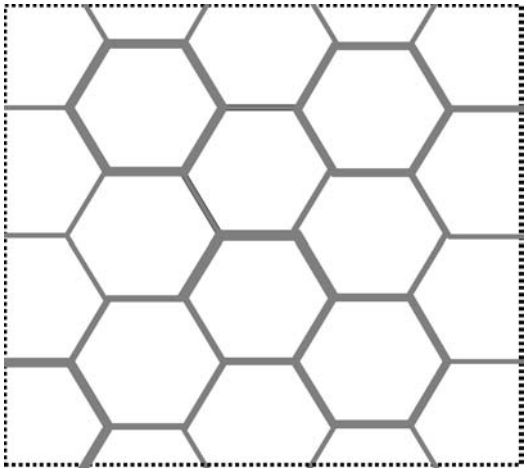

Figure 9 Schematic illustration of microstructures along the shear plane in a nano-crystal, where shaded bands correspond to boundary regions.

There is still no theory that can describe the entire range of the behavior depicted in Fig. 8, several simple models, however, have recently been proposed to understand the reverse Hall-Petch effect, in which the triple junction volume, the size-dependent line tension, and different deformation modes were considered [66–69]. For example, Masumura *et al*. [70] assumed that polycrystals with coarse-grains obey the classical Hall-Petch relation in Equation 7, and for very fine grains, the enhanced grain boundary diffusion (Coble creep) is active and the yield stress σ_y *versus* grain diameter d is given by:

$$\sigma_y = \frac{Gb}{d} + Bd^3 \tag{9}$$

where B is Coble constant which is temperature and strain-rate dependent [71]. It is further assumed that there is a critical grain size d_c at which value the Hall-Petch relation switches to Coble creep based on the presence of highly disordered grain boundaries [72]. The analytical results compared well with experimental data from Cu and NiP. The experimental evidence, however, is still lacking for which the reverse Hall-Petch effect should be very sensitive to temperature if the Coble creep mechanism is correct.

Fig. 9 illustrates the sectional microstructure of a nanocomposite coating along a shear plane, on which shear deformation is composed of grain boundary sliding. The shaded bands indicate the boundary region of which the width t varies from one boundary to another and its average is αt (here, α is about 2) [73]. Along the shear front, the fraction of boundary region is $\alpha t/d$ and that of crystalline region is $(1-\alpha t/d)$. Suppose that the stresses propagate the shear front in the boundary region and in the crystalline matrix are σ_b and σ_c respectively, the stress necessary to propagate the shear front, which is approximately proportional to hardness, can be written as:

$$\sigma = \sigma_c - \frac{\alpha t}{d}(\sigma_c - \sigma_b) \tag{10}$$

In most cases, $\sigma_c > \sigma_b$, hence, as the grain boundary region increases the stress or hardness decreases, leading to the reverse Hall-Petch relationship.

Recent investigations suggested that the hardening mechanisms of nc-TiN/a-Si_3N_4 nano-composite coatings involve two independent factors: the size-dependent yield strength as discussed above and the morphology of nc-TiN grains like the aspect ratio ρ (= length/width) [74]. With an increase of silicon content, the columnar structures of coatings gradually transfer to elongated grains with small aspect ratio, as schematically illustrated in Fig. 10. To correlate hardness with microstructures, a 2-dimensional microstructural model was proposed based on the work by Gao *et al*. [75], see inset in Fig. 10g.

Elastic-plastic finite element simulations were performed on a unit cell, in which the stress-strain relationships of nc-TiN and a-SiN_x were modeled by Hooke's law and the yield stress of nc-TiN was assumed to be dependent on the grain size. It is further assumed that the nc-TiN/a-SiN_x nanocomposite yields if the effective stress in one of the two constitutes reaches its yield strength. Simulation results showed that, in the optimal regime of 4.5 at.% Si content and the aspect ratio $\rho \approx 3$ of nc-TiN grains, the microstructure combines mechanical confinement effects with load transfer between the two phases of nc-TiN and a-SiN_x (see Fig. 10) [74]. Here, it is worth noting that the optimal content of silicon in nc-TiN/a-Si_3N_4 nano-composites is closely related to their deposition conditions. Hardness was reported to reach a maximum of 50–60 GPa at silicon content of about 8–10 at.% when the nano-crystals were covered with about one mono-layer of silicon [3, 44]. In contrast to that shown in Fig. 10, the columnar structure vanishes when superhard nanocomposites with the optimal composition are formed [3].

For the same class of nanocomposite coatings, distinctly different microstructures were also observed at the optimal silicon content as demonstrated in Fig. 11. The high hardness regime in the 3–5 nm grain size range is thought to be controlled by the as-formed new amorphous phase, which acts as a barrier to dislocation motions, in a 2-phase material comprising nanocrystalline TiN and amorphous Si_3N_4 [76]. Similar behavior was also noticed in nc-TiN/a-TiB_2 coatings, whose 2-phase morphology is clearly seen in Fig. 12 [13].

Thus, the relationships between the microstructures of superhard coatings and hardness are still an unsolved problem, and more studies are needed.

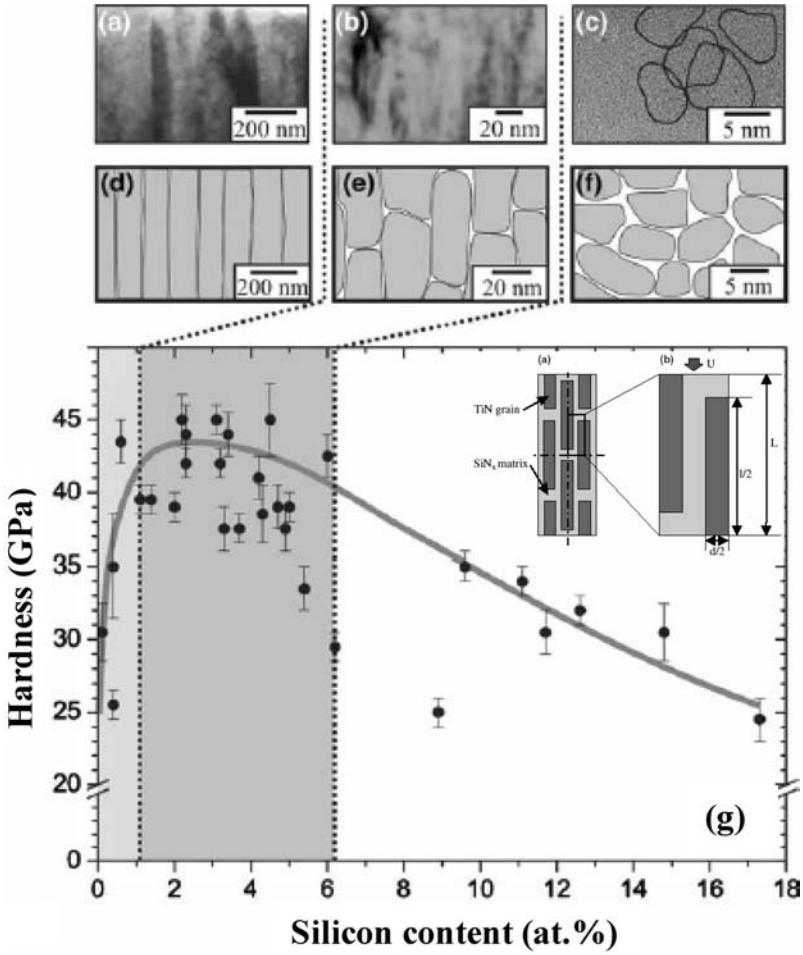

Figure 10 (a)–(c) TEM images of nc-TiN/a-SiN_x contains with 0.6, 4.7, and 11 at.% silicon content and (d)–(f) their corresponding schematic microstructures, respectively. (g) Experimental hardness *versus* Si content, and the inset shows the representative volume and unit cell models for the coatings, where L is the length of a unit cell, U is the compressive displacement of the cell, l and d are the length and width of TiN grains, respectively [74].

3.2. Atomistic scale models and simulation

Relative to strength, a measure of the resistance of a solid against failure, hardness is the resistance against local plastic deformation, microscopically corresponding to the motion of dislocations. Thus, a hard or superhard nanocomposite coating must also resist fracture to be useful in applications. As shown in Fig. 1, hard coatings are characterized by large plastic deformation, but superhard coatings are characterized by high elastic recovery. In nano-composite coatings, as the grain size of nano-crystallites is reduced to several nanometers, dislocation activities will be hindered in deformation processes [60, 64]. Instead, shear band formation in the amorphous phase, partial dislocation emission from the interface and deformation twinning in nano-crystallites may be of importance (see Fig. 8). Using high-resolution transmission electron microscopy (TEM) and associated techniques, experimental studies on the deformation mechanisms of nano-crystals with grain sizes in the nanometer range have recently gained a great deal of attention [59]. As the result of nano-scale and interface effects, several peculiar deformation mechanisms, different from dislocation pile-up, have been observed in nanocrystalline metals, such as rotational deformation (disclination dipoles) in nanocrystalline iron [77, 78], deformation twinning in nanocrystalline aluminum [79], and grain boundary-mediated plasticity in nanocrystalline nickel [80, 81]. However, TEM requires samples to be thinned down to a thickness comparable to the grain size, which can induce structural relaxation and change of grain boundary structures. At the same time, due to the difficulties in preparing high-quality samples, experimental observation remains controversial in many aspects. To-date, there is lack of a visualization technique that allows non-intrusive investigation of grain boundary structures during deformation.

With the rapid development of massively parallel computing techniques, atomic-level simulations, such as lattice statics/dynamics, Monte Carlo and especially molecular dynamics, shed light on the study of deformation mechanisms and provide novel insights into the structural and mechanical behavior of nanocrystalline materials, which is usually not available from experiments

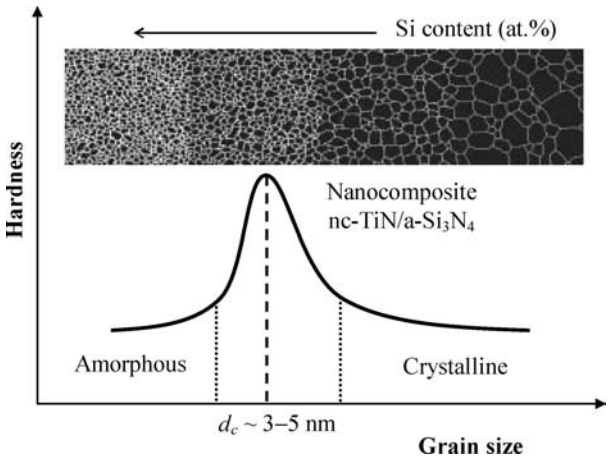

Figure 11 Illustration of hardness *versus* grain size for nc-TiN/a-Si_3N_4 coatings. The inset shows the microstructure evolution as the increase of Si content (at.%).

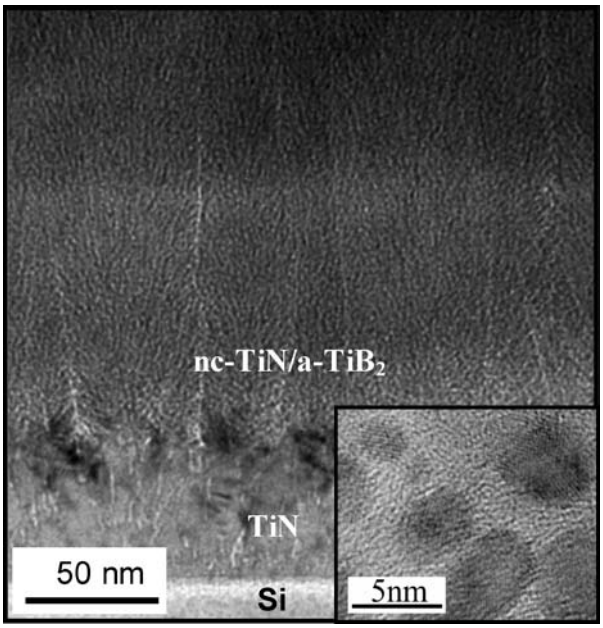

Figure 12 Nanocrystalline TiN grains (~ 4-5 nm) embedded in a thin matrix of amorphous TiB_2 observed by high resolution TEM [13].

[59]. One well-known example is the theoretically predicted material β-C_3N_4 with hardness comparable to that of diamond [82]. Recently, to simulate the plastic deformation of nanocrystalline copper, molecular dynamics simulations with a system size up to 100 million atoms were carried out. The results indicated that the flow strength exhibits a maximum at a grain size of 10 to 15 nanometers due to a shift in the microscopic deformation mechanism from dislocation-mediated plasticity in coarse-grained materials to grain boundary sliding in nanocrystalline regions [62, 63]. In terms of first-principle calculations, a mechanism was proposed to enhance the hardness of multilayer coatings through restricting dislocation movement in transition metal carbides by phase stability tuning, which is contrary to conventional superlattices [83]. Molecular dynamics simulations have also been widely applied in the study of tribological properties of thin films at the atomic scale [84].

Based on the idea that the intrinsic hardness of covalent crystals is equivalent to the sum of resistance to the indenter of each bond per unit area, a semi-empirical formula to predicting the hardness (in the unit of GPa) of a material was recently given by Gao *et al*. [85]:

$$H = 350\frac{N_e^{2/3}e^{-1.191f_i}}{d^{2.5}} \tag{11}$$

where N_e is electron density expressed in the number of valence electrons per cubic angstroms (Å), f_i is ionicity of chemical bond, and d is bond length in Å. As to a superhard material, three conditions should be met: higher bond or electronic density, shorter bond length, and greater degree of covalent bonding [85]. Carbon in its diamond polymorph meets the best combination of these conditions, and has the highest value of elastic modulus and hardness [86, 87]. This semi-empirical formula also makes a connection between the hardness and first-principle or *ab initio* calculation and is instructive to the study of hardening mechanisms [85]. However, since their work is based on the fact that atomic bonds are broken in the process of an indentation, it is difficult to estimate the hardness of nanocomposite coatings quantitatively only by elastic parameters like bulk or shear modulus. A recent study based on the density functional theory showed that the theoretical fracture toughness, $K \sim (\gamma_s G)^{1/2}$, where γ_s is the surface energy and G is shear modulus, may be used to characterize the hardness of diamond and other brittle materials [88]. According to Kisly [89], the work done during an indentation includes four components: elastic deformation, plastic deformation, formation and propagation of cracks, and creation of new surfaces. Thus, the hardness of a material depends on its bond energy, bond covalence and bond length. In addition, the parameters describing plastic deformation and fracture, such as Burgers vector, distance between neighboring slip planes and critical crack length etc., are also of importance. Following the semi-empirical formula of Equation 11, the hardening mechanisms of nano-crystalline Ti-Al-N solid solution films were investigated [90]. The calculation revealed that both intrinsic hardening and grain boundary hardening had a negligible contribution for the films with relatively low Al contents. As illustrated in Fig. 13, the improved hardness in Ti-Al-N coatings originates primarily from the effect of solid solution hardening.

Although these explanations for the superhardness of nanocomposite coatings, in either macro- or atomic-scales, are rather qualitative and concrete evidence is somewhat lacking, the elevated hardness coincides with a

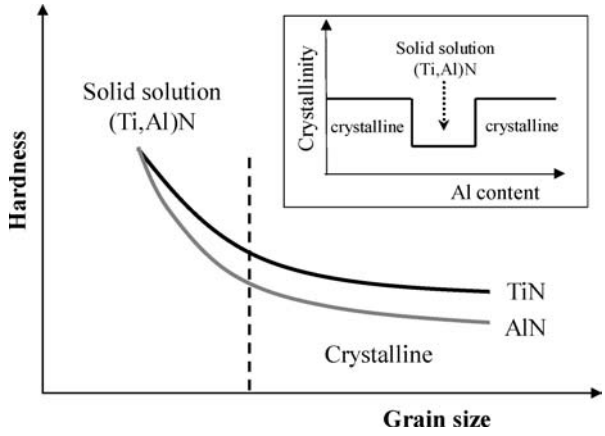

Figure 13 Illustration of hardness *versus* grain size for (Ti, Al)N solid solution. The inset shows the change of crystallinity with increase of Al content.

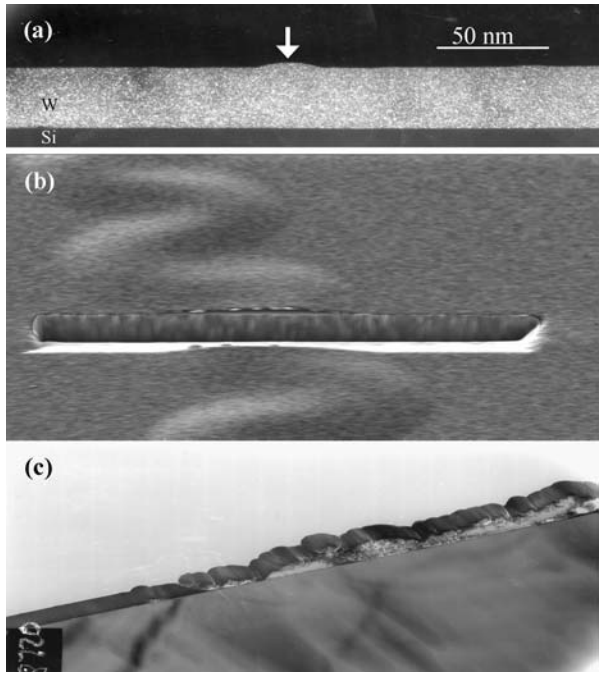

Figure 14 (a) Dark-fields cross-sectional TEM image of a region showing the onset of buckling in a compressed W thin films on Si(100) substrate. (b) Cross-sectional image using focused ion beam analysis of the region from a buckled telephone cord-like film. (c) Bright-field cross-sectional TEM image showing a part of the film peeled off from the substrate.

reduced grain size or a high density of grain boundaries. As shown in Fig. 11, hardness enhancement of nc-TiN/a-Si_3N_4 nanocomposite coatings is due to strong restraint imposed by the amorphous SiN_x phase on the growth of the nanocrystalline TiN grains. A modified Monte Carlo Potts model for the grain growth of single-phase films was used to simulate $Ti_{1-x-y}Si_xN_y$ systems [51]. The simulation results showed that amorphous SiN_x prefers to adhere to TiN grain-boundary due to the driving force caused by the energy difference between TiN grain-boundary energy and TiN/SiN_x interfacial energy, and the SiN_x matrix can lead to a remarkable decrease of TiN grain sizes [51].

3.3. Multi-scale modeling

Although atomistic simulations have reached a level that some mechanical behavior ahead of experiments can be estimated, most simulations of deformation processes are only performed under much higher stresses and much shorter deformation times than in experiments. Under longer deformation times, many other processes take place in the grain boundary of nano-materials that may change their microstructures during the deformation. The buckling and delamination process of nanocomposite coatings is a typical evolving and non-local damage process with multi-scale nature as shown in Fig. 14. Here, let us use nanoindentation fracture as an example, The fracture of a coating/substrate system can be viewed as three main stages (see Fig. 15): the first ring-like through-thickness crack formation, delamination and buckling around the contact area, and the second ring-like through-thickness crack formation and spallation [43]. Fig. 16 shows the images of four nc-TiN/a-Si_3N_4 coatings indented to different loads using a 5 μm radius spherically tipped nanoindenter [55]. Thus, it is necessary to develop methods which can model material properties across several length-scales. Roughly, attempts on multi-scale modeling can be divided into two aspects: one is to link simulation methods used at different scales and the other is to find the so-called universal properties that are independent of microscopic and macroscopic details.

Recent studies have coupled atomic-scale simulations to finite element modeling to investigate dislocations [91]. Compared to conventional finite element analysis, the material point method (MPM) may be a good candidate in the study of film delamination and pattern formation during a nanoindentation process, and further provide a better understanding on the underlying physics [92]. MPM is a mesh-less method, in which a solid body is discretized to a collection of points as shown in Fig. 17 [16]. In this method, the combination of Lagrangian and Eulerian descriptions has proved useful for solving solid mechanics problems including those with large deformations and rotations. Moreover, MPM may also bridge finite element analysis and molecular dynamics for multi-scale modeling. To show the potential of the method, a parametric study was conducted to explore the effects of aspect ratio and failure mode on the evolution of failure patterns in superhard coatings under various loading and boundary conditions [93].

Nanocomposite coatings subjected to external stress display bursts of activity due to the nucleation and motion of dislocations and cracks, buckling, and delamination. This so-called crackling noise can be directly monitored and recorded by an acoustic emission (AE) sensor. A

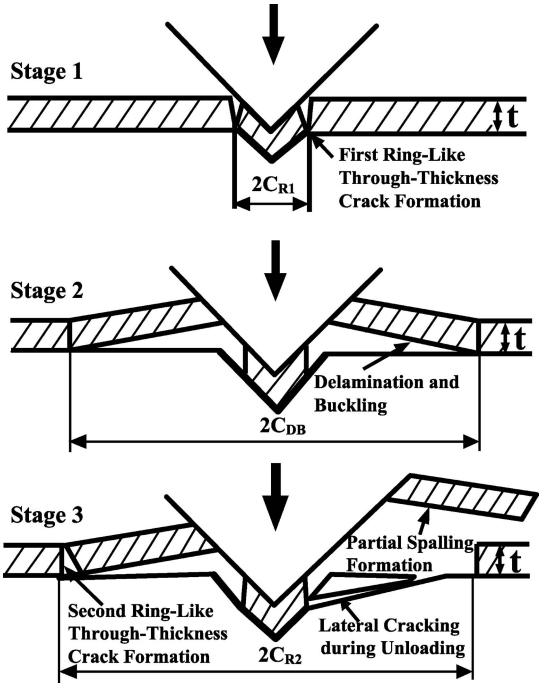

Figure 15 Schematics of the three stages in nanoindentation fracture of a coating/substrate system [43].

wide range of physical systems exhibiting crackling noise have been studied in the last decade or so, and some universal behavior has been discovered over a huge range of sizes [94]. As a nanocomposite coating approaches an optimal performance, the AE energy-frequency follows a power-law distribution (see Fig. 18), that is, its mechanical behavior is likely to be independent of microscopic and macroscopic details. Recently, AE signals due to scratching superhard nc-TiN/a-Si_3N_4 coatings were studied using a simple stick-slip model. The optimal information extracted from statistical analysis such as Si content, deposition temperature etc., in terms of an entropy maximum principle [95, 96], is in good agreement with the nanoindentation and machining tests. The results imply that a better understanding of the origin of superhardness may rely on only a few emergent material parameters that describe the competition between differ-

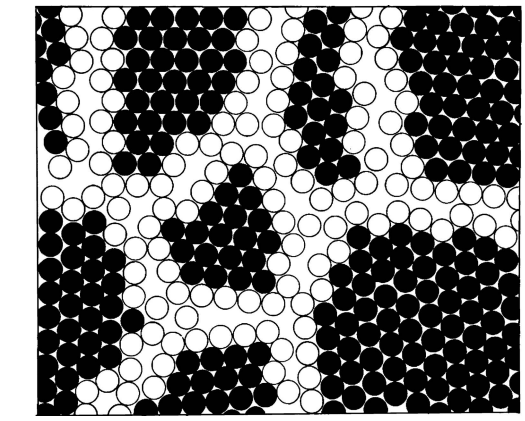

Figure 17 Two-dimensional model of a nanostructured material. The atoms in the centres of crystals and the boundary core regions are represented as black and open circles, respectively [16].

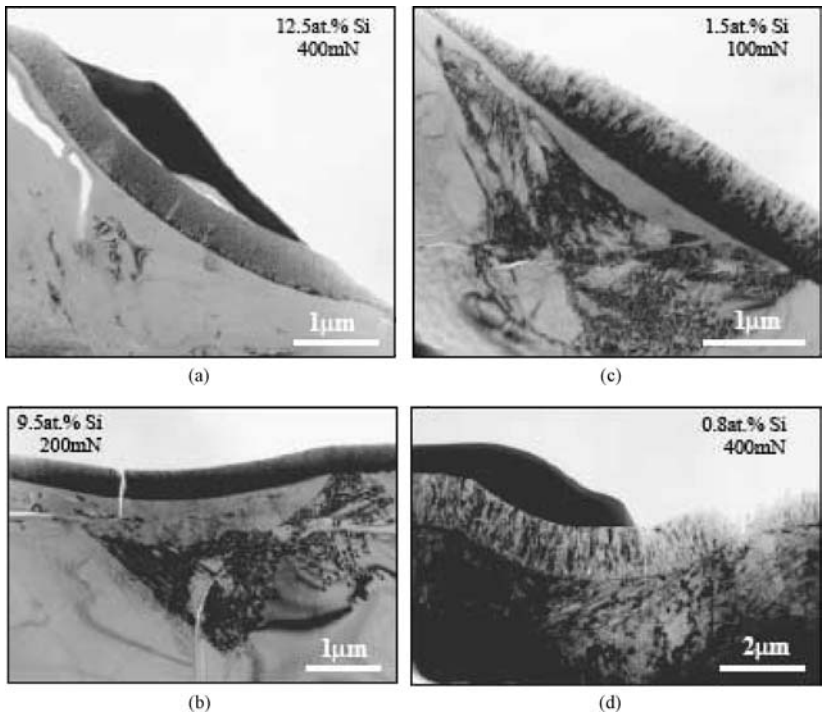

Figure 16 Images of four nc-TiN/a-Si_3N_4 coatings indented to different loads using a 5 μm radius spherically tipped nanoindenter [55].

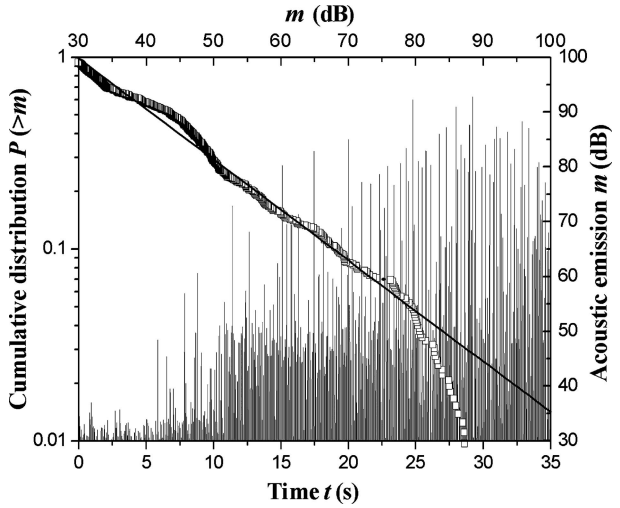

Figure 18 AE signals from the scratching test on nc-TiN/a-Si_3N_4 coatings (8.6 at.% Si and 400°C deposition temperature) *versus* time and the cumulative frequency-magnitude distribution $P(>m)$ of AE events with magnitude greater than m, where the slope of the solid line is −0.026 [97].

ent deformation mechanisms such as dislocation pile-up in nano-crystalline grains and sliding/rotation of grains within amorphous boundaries, or mechanical confinement effects and optimal load transfer between phases. Using superhard nc-TiN/a-Si_3N_4 coatings as an example, the nc-TiN phase is sufficiently hard to bear the load whilst the a-Si_3N_4 phase provides structural flexibility, in which further increase in hardness requires blocking of grain-boundary sliding by optimal design of their microstructures [74, 97]. It is this competition that causes the unique mechanical properties of superhard nanocomposite coatings.

4. Conclusions

For nanocomposite coatings to be superhard, three conditions should be met in the viewpoint of continuum mechanics: high bulk modulus, high shear modulus, and low density of flaws (nano-cracks or dislocations). The corresponding conditions at the atomistic scale are: higher bond or electronic density, shorter bond length, and greater degree of covalent bonding. There have been great advances in making connections between the macroscopic properties and atomistic- or nano-structures. But our basic understanding of the origin of superhardness is far from complete and many open questions remain. To tailor and optimize the mechanical behavior like the hardness of nanocomposite coatings, one of the most important aspects is to untangle their underlying mechanisms. Much more research is needed on experimental observations at the nano-scale, theoretical modeling and computer simulations. The following aspects are worthy of further systematic investigations:

- study methods for hardness measurement of superhard, especially ultrahard, coatings including influences of size effect, substrate, tip roundness, residual stresses etc;
- develop correlations between nanostructures and their mechanical properties such as hardness;
- establish via both experiments and mechanics modeling the deformation mechanisms of nanostructured materials;
- identify the intrinsic origin of the superhardness of nanocomposite coatings; and
- explore approaches and techniques to link simulation methods at different scales.

Acknowledgements

This work is supported by both the Australian Research Council (ARC) and the Hong Kong SAR Research Grant Council (Project No. CityU 1132/03E). YWM and CL are, respectively, Australian Federation Fellow and ARC Senior Research Associate at the Centre for Advanced Materials Technology, the University of Sydney. We are also grateful to our colleagues in the University of Sydney and the City University of Hong Kong for their inputs in the form of original artwork and technical discussions that are an integral part of this review article.

References

1. W. KULISCH, "Deposition of diamond-like superhard materials" (Springer, Berlin; London, 1999).
2. S. C. TJONG and H. CHEN, *Mater. Sci. Eng. R-Rep.* **45** (2004) 1.
3. S. VEPREK, M. G. J. VEPREK-HEIJMAN, P. KARVANKOVA and J. PROCHAZKA, *Thin Solid Films* **476** (2005) 1.
4. G. E. FOUGERE, L. RIESTER, M. FERBER, J. R. WEERTMAN and R. W. SIEGEL, *Mater. Sci. Eng. A* **204** (1995) 1.
5. R. W. CAHN, *Nature* **380** (1996) 104.
6. V. V. BRAZHKIN, A. G. LYAPIN and R. J. HEMLEY, *Philos. Mag. A* **82** (2002) 231.
7. S. VEPREK, *J. Vac. Sci. Technol. A* **17** (1999) 2401.
8. J. HAINES, J. M. LEGER and G. BOCQUILLON, *Ann. Rev. Mater. Res.* **31** (2001) 1.
9. J. MUSIL, *Surf. Coat. Technol.* **125** (2000) 322.
10. S. ZHANG, D. SUN, Y. Q. FU and H. J. DU, *ibid.* **167** (2003) 113.
11. W. D. SPROUL, *Science* **273** (1996) 889.
12. T. FU, Z. F. ZHOU, K. Y. LI and Y. G. SHEN, *Mater. Lett.* **59** (2005) 618.
13. Y. H. LU, P. SIT, H. F. HUNG, H. D. CHEN, Z. F. ZHOU, K. Y. LI and Y. G. SHEN, *J. Vac. Sci. Technol. B* **23** (2005) 449.
14. P. F. MCMILLAN, *Nature* **430** (2004) 738.
15. A. ROSENFLANZ, M. FREY, B. ENDRES, T. ANDERSON, E. RICHARDS and C. SCHARDT, *ibid.* **430** (2004) 761.
16. H. GLEITER, *Prog. Mater. Sci.* **33** (1989) 223.
17. *Idem.*, *Acta Mater.* **48** (2000) 1.
18. D. TABOR, "The Hardness of Metals" (Clarendon Press, Oxford, 1951).
19. D. TABOR, *Philos. Mag. A* **74** (1996) 1207.

20. A. C. FISCHER-CRIPPS, "Nanoindentation" (Springer, New York, 2002).
21. W. C. OLIVER and G. M. PHARR *J. Mater. Res.* **7** (1992) 1564.
22. *Idem., ibid.* **19** (2004) 3.
23. V. BRAZHKIN, N. DUBROVINSKAIA, A. NICOL, N. NOVIKOV, R. RIEDEL, R. SOLOZHENKO and Y. ZHAO, *Nat. Mater.* **3** (2004) 576.
24. N. JIANG, Y. G. SHEN, Y.-W. MAI, T. CHAN and S. C. TUNG, *Mater. Sci. Eng. B* **106** (2004) 163.
25. W. D. NIX and H. J. GAO, *J. Mech. Phys. Solids* **46** (1998) 411.
26. T. Y. ZHANG and W. H. XU, *J. Mater. Res.* **17** (2002) 1715.
27. J. MUSIL, H. ZEMAN, F. KUNC and J. VLCEK, *Mater. Sci. Eng. A* **340** (2003) 281.
28. S. VEPREK, S. MUKHERJEE, H. D. MANNLING and J. L. HE, *ibid.* **340** (2003) 292.
29. K. J. JOHNSON, "Contact Mechanics" (Cambridge University Press, Cambridge, 1985).
30. S. VEPREK and A. S. ARGON, *J. Vac. Sci. Technol. B* **20** (2002) 650.
31. J. L. HE and S. VEPREK, *Surf. Coat. Technol.* **163** (2003) 374.
32. N. A. FLECK and J. W. HUTCHINSON, *Adv. Appl. Mech.* **33** (1997) 295.
33. I. YONENAGA, T. SHIMA and M. H. F. SLUITER, *Jpn. J. Appl. Phys.* **41** (2002) 4620.
34. C. LU, Y.-W. MAI and Y. G. SHEN, *Key Eng. Mater.* **312** (2006), 363.
35. S. M., JEONG, P. M. SHUM, Y. G. SHEN, K. Y. LI, Y.-W. MAI and H. L. LEE, *J. Mater. Sci.* (2005), submitted.
36. Y. G. SHEN, Y.-W. MAI, D. R. MCKENZIE, Q. C. ZHANG, W. D. MCFALL and W. E. MCBRIDE, *J. Appl. Phys.* **88** (2000) 1380.
37. Y. G. SHEN, Y.-W. MAI, Q. C. ZHANG, D. R. MCKENZIE, W. D. MCFALL and W. E. MCBRIDE, *ibid.* **87** (2000) 177.
38. G. C. STONEY, *Proc. R. Soc. London A* **82** (1909) 172.
39. S. HAYASHI, T. HIRAI, K. HIRAGA and M. HIRABAYASHI, *J. Mater. Sci.* **17** (1982) 3336.
40. V. VALVODA, R. KUZEL, R. CERNY and J. MUSIL, *Thin Solid Films* **156** (1988) 53.
41. W. HERR and E. BROSZEIT, *Surf. Coat. Technol.* **97** (1997) 335.
42. F. KAUFFMANN, G. DEHM, V. SCHIER, A. SCHATTKE, T. BECK, S. LANG and E. ARZT, *Thin Solid Films* **473** (2005) 114.
43. B. BHUSHAN, *Diam. Relat. Mat.* **8** (1999) 1985.
44. S. VEPREK and S. REIPRICH, *Thin Solid Films* **268** (1995) 64.
45. J. H. ROSE, J. R. SMITH, F. GUINEA and J. FERRANTE, *Phys. Rev. B* **29** (1984) 2963.
46. S. VEPREK, S. MUKHERJEE, P. KARVANKOVA, H. D. MANNLING, J. L. HE, K. MOTO, J. PROCHAZKA and A. S. ARGON, *J. Vac. Sci. Technol. A* **21** (2003) 532.
47. R. HILL, "The Mathematical Theory of Plasticity" (Oxford University Press, 1950).
48. P. MARSH, *Proc. R. Soc. London A* **279** (1964) 420.
49. G. I. BARENBLATT, "Scaling" (Cambridge University Press, Cambridge, 2003).
50. Y. T. CHENG and C. M. CHENG, *Mater. Sci. Eng. R-Rep.* **44** (2004) 91.
51. Z. J. LIU, C. H. ZHANG, Y. G. SHEN and Y.-W. MAI, *J. Appl. Phys.* **95** (2004) 758.
52. S. VEPREK and A. S. ARGON, *Surf. Coat. Technol.* **146** (2001) 175.
53. S. VEPREK, S. MUKHERJEE, P. KARVANKOVA, H. D. MANNLING, J. L. HE, K. MOTO, J. PROCHAZKA and A. S. ARGON, *Thin Solid Films* **436** (2003) 220.
54. S. VEPREK, S. REIPRICH and S. H. LI, *Appl. Phys. Lett.* **66** (1995) 2640.
55. J. M. CAIRNEY, M. J. HOFFMAN, P. R. MUNROE, P. J. MARTIN and A. BENDAVID, *Thin Solid Films* **479** (2005) 193.
56. A. A. GRIFFITH, *Phil. Trans. Roy. Soc. London* **221** (1921) 163.
57. E. O. HALL, *Proc. Phys. Soc. London B* **64** (1951) 747.
58. N. J. PETCH, *J. Iron Steel Inst.* **174** (1953) 25.
59. D. WOLF, V. YAMAKOV, S. R. PHILLPOT, A. MUKHERJEE and H. GLEITER, *Acta Mater.* **53** (2005) 1.
60. S. YIP, *Nat. Mater.* **3** (2004) 11.
61. *Idem., Nature* **391** (1998) 532.
62. J. SCHIOTZ, F. D. DI TOLLA and K. W. JACOBSEN, *ibid.* **391** (1998) 561.
63. J. SCHIOTZ and K. W. JACOBSEN, *Science* **301** (2003) 1357.
64. H. VAN SWYGENHOVEN, *ibid.* **296** (2002) 66.
65. T. R. SMITH, R. W. ARMSTRONG, P. M. HAZZLEDINE, R. A. MASUMURA and C. S. PANDE (Eds.) "Grain Size and Mechanical Properties — Fundamentals and Applications," (Materials Research Society, Pittsburgh, 1995) Vol. 362.
66. G. PALUMBO, S. J. THORPE and K. T. AUST, *Scr. Metall. Mater.* **24** (1990) 1347.
67. C. SURYANARAYANA, D. MUKHOPADHYAY, S. N. PATANKAR and F. H. FROES, *J. Mater. Res.* **7** (1992) 2114.
68. R. O. SCATTERGOOD and C. C. KOCH, *Scr. Metall. Mater.* **27** (1992) 1195.
69. V. G. GRYAZNOV and L. I. TRUSOV, *Prog. Mater. Sci.* **37** (1993) 289.
70. R. A. MASUMURA, P. M. HAZZLEDINE and C. S. PANDE, *Acta Mater.* **46** (1998) 4527.
71. R. L. COBLE, *J. Appl. Phys.* **34** (1963) 1679.
72. V. YAMAKOV, D. WOLF, S. R. PHILLPOT and H. GLEITER, *Acta Mater.* **50** (2002) 61.
73. S. TAKEUCHI, *Scr. Mater.* **44** (2001) 1483.
74. F. KAUFFMANN, B. H. JI, G. DEHM, H. J. GAO and E. ARZT, *ibid.* **52** (2005) 1269.
75. H. J. GAO, B. H. JI, I. L. JAGER, E. ARZT and P. FRATZL, *Proc. Natl. Acad. Sci. USA.* **100** (2003) 5597.
76. C. H. ZHANG, Z. J. LIU, K. Y. LI, Y. G. SHEN and J. B. LUO, *J. Appl. Phys.* **95** (2004) 1460.
77. M. MURAYAMA, J. M. HOWE, H. HIDAKA and S. TAKAKI, *Science* **295** (2002) 2433.
78. I. A. OVID'KO, *ibid.* **295** (2002) 2386.
79. M. W. CHEN, E. MA, K. J. HEMKER, H. W. SHENG, Y. M. WANG and X. M. CHENG, *ibid.* **300** (2003) 1275.
80. Z. W. SHAN, E. A. STACH, J. M. K. WIEZOREK, J. A. KNAPP, D. M. FOLLSTAEDT and S. X. MAO, *ibid.* **305** (2004) 654.
81. E. MA, *ibid.* **305** (2004) 623.
82. A. Y. LIU and M. L. COHEN, *ibid.* **245** (1989) 841.
83. H. W. HUGOSSON, U. JANSSON, B. JOHANSSON and O. ERIKSSON, *ibid.* **293** (2001) 2434.
84. B. BHUSHAN, J. N. ISRAELACHVILI and U. LANDMAN, *Nature* **374** (1995) 607.
85. F. M. GAO, J. L. HE, E. D. WU, S. M. LIU, D. L. YU, D. C. LI, S. Y. ZHANG and Y. J. TIAN, *Phys. Rev. Lett.* **91** (2003) 015502.
86. J. J. GILMAN, *Philos. Mag. A* **82** (2002) 1811.
87. J. J. GILMAN, *Science* **261** (1993) 1436.
88. Z. DING, S. ZHOU and Y. ZHAO, *Phys. Rev. B* **70** (2004) 184117.
89. P. S. KISLY, *Inst. Phys. Conf. Ser.* **75** (1986) 107.
90. Z. J. LIU, P. W. SHUM and Y. G. SHEN, *Thin Solid Films* **468** (2004) 161.
91. E. B. TADMOR, M. ORTIZ and R. PHILLIPS, *Philos. Mag. A* **73** (1996) 1529.

92. Z. CHEN, W. HU, L. SHEN, X. XIN and R. BRANNON, *Eng. Fract. Mech.* **69** (2002) 1873.
93. Z. CHEN, L. SHEN, Y.-W. MAI and Y. G. SHEN, *ZAMP* **56** (2005) 908.
94. J. P. SETHNA, K. A. DAHMEN and C. R. MYERS, *Nature* **410** (2001) 242.
95. H. AKAIKE, *IEEE Trans. Autom. Control* **19** (1974) 716.
96. C. S. LU, R. DANZER and F. D. FISCHER, *Phys. Rev. E* **65** (2002) 067102.
97. C. LU, Y.-W. MAI and Y. G. SHEN, *ibid.* **72** (2005) 027101.